

Supporting Information for

Tetragonal $\text{Li}_{10}\text{GeP}_2\text{S}_{12}$ and Li_7GePS_8 – exploring the Li ion dynamics in LGPS Li electrolytes

Alexander Kuhn,^a Viola Duppel^a and Bettina V. Lotsch*^{a,b}

^a Max Planck Institute for Solid State Research, Heisenbergstr. 1, 70569 Stuttgart, Germany. E-mail: b.lotsch@fkf.mpg.de
^b Department of Chemistry, Ludwig-Maximilians-Universität München, Butenandtstr. 5-15, 81377 München, Germany.

S1 - Experimental Details

Due to the moisture and air sensitivity of the material, all preparation and analysis steps were performed under inert Ar atmosphere. XRD was performed with a STOE Stadi P diffractometer working in Debye-Scherrer geometry with Mo $K_{\alpha 1}$ radiation (Ge(111) monochromator). For the Rietveld refinement, DiffracPlus TOPAS v4.2 (Bruker AXS) was used. TEM was performed using a Philips CM30 ST (300 kV). NMR measurements were performed with Bruker Avance II spectrometers connected to cryomagnets of 9.4 T and 4.7 T. For ^{31}P MAS measurements, a Bruker 4mm-MAS probe was used (rotation rate 12 kHz). The measurements were performed with single-pulse excitation and a sufficiently long recycle delay to allow complete relaxation. For ^7Li PFG NMR, ^7Li NMR line shape, and ^7Li NMR relaxometry, a Bruker Diff60 probe was used. For the PFG measurements a stimulated echo pulse sequence with two gradient pulses of variable strength separated by the diffusion time Δ was used. Longitudinal relaxation was measured using a saturation recovery pulse sequence with 14 different delay times ($10^{-4} \dots 2.2$ s). Transversal relaxation was measured using a solid echo pulse sequence with 14 different delay times ($10^{-5} \dots 0.22$ s). The line shapes were measured with single-pulse excitation. Impedance spectroscopy was performed using a Novocontrol Alpha Analyzer and a home-built impedance cell. For the measurement, pellets (8 mm diameter, 1.5-3 mm thickness) were pressed from the powdered sample. Li-blocking Au electrodes were sputtered on the surfaces of the annealed pellets.

S2 – Details of the Rietveld refinements

The XRD patterns of $\text{Li}_{10}\text{GeP}_2\text{S}_{12}$ and Li_7GePS_8 were analyzed with Rietveld refinement on the basis of the structure of tetragonal LGPS reported in the literature.^[1] The Li positions were not subject to the refinement. The atom positions and occupancies of the heavy atoms Ge, P, and S obtained from the Rietveld refinements are listed below.

$\text{Li}_{10}\text{GeP}_2\text{S}_{12}$

radiation: Mo K $_{\alpha 1}$

space group $P4_2/nmc$ (137:1)

Tetragonal, $a = b = 8.7136(20)$ Å, $c = 12.6072(30)$ Å

Pos.	Wyck.	x	y	z	occ.	B_{eq} (Å 2)
Ge1	4d	0	0.5	0.68866(68)	0.539(16)	1.67(29)
P1	4d	0	0.5	=z(Ge1)	=1-occ(Ge1)	= B_{eq} (Ge1)
P2	2b	0	0	0.5	1	4.07(63)
S1	8g	0	0.19127(70)	0.40913(78)	1	3.14(27)
S2	8g	0	0.29818(83)	0.09661(64)	1	1.42(27)
S3	8g	0	0.69600(85)	0.79064(58)	1	1.73(29)

$R_{\text{exp}} = 5.23$, $R_{\text{wp}} = 5.42$, $R_p = 4.29$, $GoF = R_{\text{wp}} / R_{\text{exp}} = 1.04$

Li_7GePS_8

radiation: Mo K $_{\alpha 1}$

space group $P4_2/nmc$ (137:1)

Tetragonal, $a = b = 8.71825(48)$ Å, $c = 12.65972(71)$ Å

Pos.	Wyck.	x	y	z	occ.	B_{eq} (Å 2)
Ge1	4d	0	0.5	0.69029(14)	0.7412(46)	1.527(59)
P1	4d	0	0.5	=z(Ge1)	=1-occ(Ge1)	= B_{eq} (Ge1)
P2	2b	0	0	0.5	1	1.48(12)
S1	8g	0	0.185955(19)	0.40723(19)	1	2.804(77)
S2	8g	0	0.29263(23)	0.09545(17)	1	1.673(71)
S3	8g	0	0.70183(21)	0.79305(16)	1	1.593(74)

$R_{\text{exp}} = 2.06$, $R_{\text{wp}} = 2.54$, $R_p = 2.02$, $GoF = R_{\text{wp}} / R_{\text{exp}} = 1.23$

[1] A. Kuhn, J. Koehler, B. V. Lotsch, *Phys. Chem. Chem. Phys.* 2013, **15**, 11620.

S3 - Comment on long-range self-diffusion in a 1D conductor and PFG NMR

^7Li PFG NMR is sensitive to Li self-diffusion on the micron scale. However, can ideal 1D single-file diffusion of ions principally be observed by ^7Li PFG NMR? To be observed in PFG NMR, individual Li ions need to migrate over large distances (several microns, see Fig. 1A). For single-file diffusion of charged particles such as Li ions, this would lead to a significant charge separation (see Fig. 1B). In MD simulations, usually, periodic boundary conditions are used. These feed in an ion which has left the box at the other side of the box in order to keep the number of atoms in the box constant (see Fig. 1C). Then, charge separation does not occur and long-range diffusion can be observed.

Thus, single-file 1D processes observed in MD simulations with periodic boundary conditions are not expected to be observed in PFG NMR measurements where self-diffusion is measured. In a quasi-1D conductor, when inter-channel hopping occurs in the material, long-range self-diffusion along the 1D axis can occur on the time scale of inter-channel diffusion. Thus, we expect that long-range self-diffusion which is probed by PFG NMR is isotropic even for a 1D conductor.

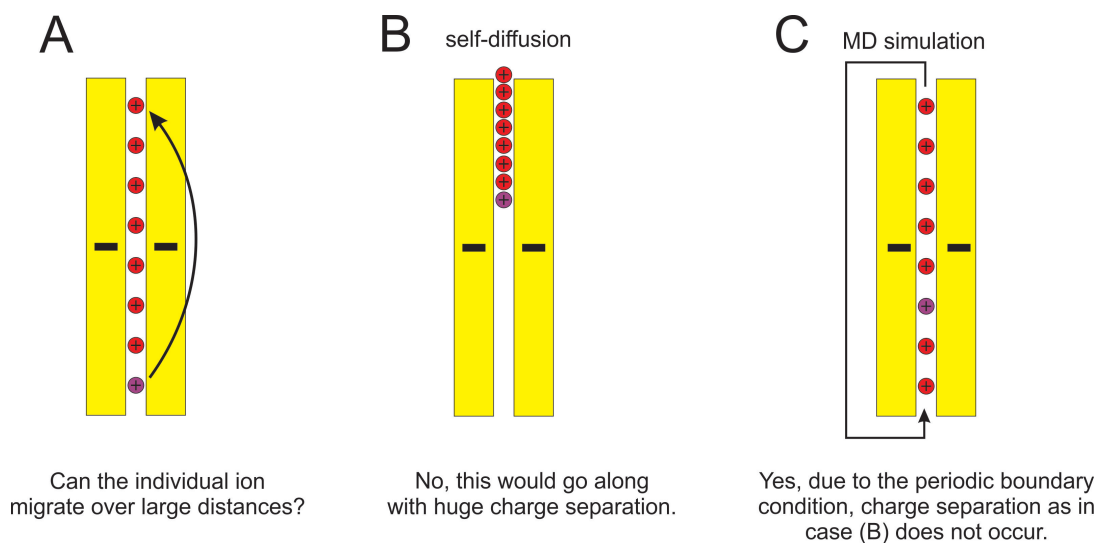


Fig. 1: Long-range transport in a 1D ion conductor.

S4 - diffusion time dependence of ${}^7\text{Li}$ NMR PFG NMR

In PFG NMR on microcrystalline solids, finite crystallite effects have to be considered when the square root of the mean square displacement $\langle x^2 \rangle(\Delta)$ with the diffusion time Δ (see pulse sequence Fig. 2A) is no longer much smaller than the crystallite size. In our measurements we set the diffusion time short enough to avoid finite crystallite effects (range marked blue in Fig. 2B). Then, the intracrystalline diffusion is measured. In this range, the echo transients followed the behavior expected for isotropic diffusion.[2] For longer diffusion times, the apparent diffusion coefficient was lower and the transients no longer followed Stejskal-Tanner behavior. This is expected for non-spherical microcrystallites. Deviations from Stejskal-Tanner behavior may generally also stem from anisotropic diffusion *within* a crystallite, but preferred single-file 1D diffusion of ions cannot be observed in PFG NMR measurements as discussed above (see section S2). Thus, we attribute the deviations from Stejskal-Tanner behavior at longer diffusion times to finite crystallite effects.

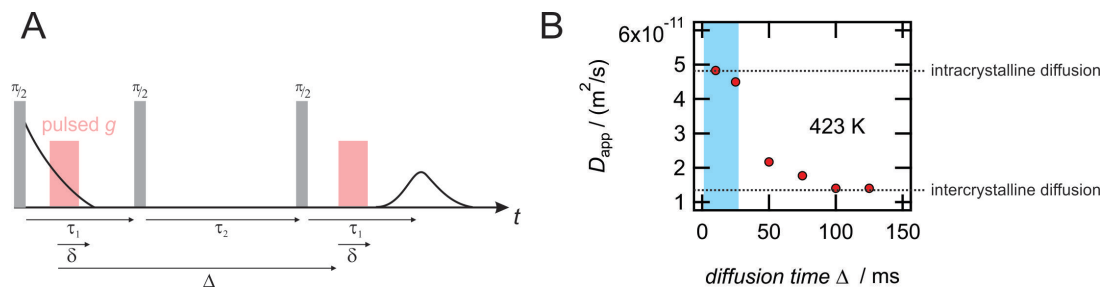


Fig. 2: Diffusion time dependence of the apparent diffusion coefficient (Li_7GePS_8).

S5 – Details of the ^7Li NMR relaxometry study

Fig. 3 summarizes the results of the NMR relaxometry study. In order to probe the Li ion dynamics on different time scales, both the longitudinal (sensitive to fast motion) and transversal NMR relaxation (sensitive to slow motion) was measured over a wide temperature range. Longitudinal relaxation was measured using a saturation recovery pulse sequence with 14 different delay times ($10^{-4} \dots 2.2$ s). Transversal relaxation was measured using a solid echo pulse sequence with 14 different delay times ($10^{-5} \dots 0.22$ s). While the longitudinal relaxation followed single exponential behaviour within the accuracy of the measurement (described by the rate R_1), the transversal relaxation could be roughly described by a sum of two exponentials (with the rates R_{2q} and R_{2d}) reflecting the time scales of quadrupolar and dipolar interaction. Let us first consider the temperature dependence of R_1 which was measured at two different external fields $B_0 = 4.7$ T (full circles) and $B_0 = 9.4$ T (empty circles). $R_1(T)$ measured at an external field B_0 surpasses a maximum when the maximum condition $\tau^{-1} \approx \omega_0 = \gamma B_0$ is fulfilled for the Li jump rate.[3] The jump rates extracted from the R_1 maxima are included in Fig. 4 as red points in the top section. At room temperature the mean Li jump rates are on the order of $\tau^{-1} \approx 10^9$ s $^{-1}$. As mentioned above, the transversal relaxation rates R_{2q} (full triangles) and R_{2d} (open triangles) are sensitive to much slower dynamics occurring on the time scale of the quadrupolar and dipolar coupling, respectively. At low temperatures, the rigid-lattice values of R_{2q} and R_{2d} are observed. Using the narrowing condition $\tau^{-1} \approx \sqrt{M_{2\text{rigid lattice}}} = \sqrt{2} \times R_{2\text{rigid lattice}}$,[3] two jump rates are extracted and included into Fig. 3 as red points. The four jump rates extracted from the NMR relaxometry measurements nicely follow an Arrhenius law with an activation energy of 0.22(1) eV (red regression line) and an attempt frequency of $\tau^{-1} \approx 2 \times 10^{12}$ s $^{-1}$. The black dashed line showing a slope of -0.22 eV indicates a quadrupolar relaxation mechanism for R_1 (rather than a dipolar one since it crosses R_{2q} (and not R_{2d}) at the narrowing condition.

[2] E. O. Stejskal, J. E. Tanner, *J. Chem. Phys.* 1965, **42**, 288.

[3] N. Bloembergen, E. M. Purcell, R. V. Pound, *Phys. Rev.* 1948, **73**, 679.

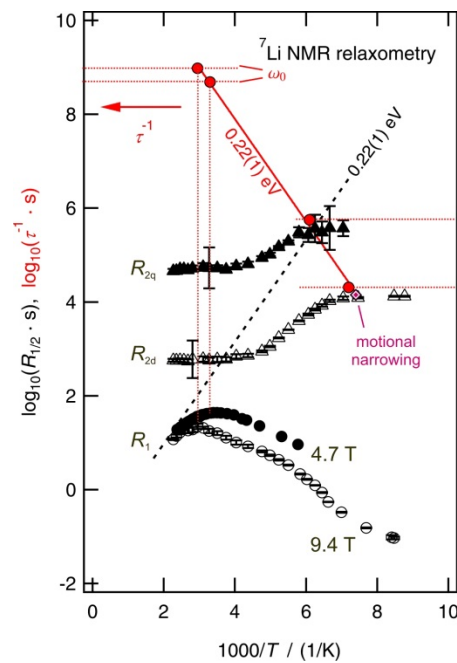


Fig. 3: ${}^7\text{Li}$ NMR relaxometry on Li_7GePS_8 . Open (full) circles: longitudinal relaxation rates measured at 9.4 (4.7) T. Open (full) triangles: dipolar (quadrupolar) transversal relaxation rates. Red points: jump rates deduced from the maximum (R_1) and narrowing (R_2) conditions. The jump rate deduced from the line narrowing (see main article) is added to the figure as well.

S6 – Impedance spectroscopy: separating grain boundary and bulk contribution:

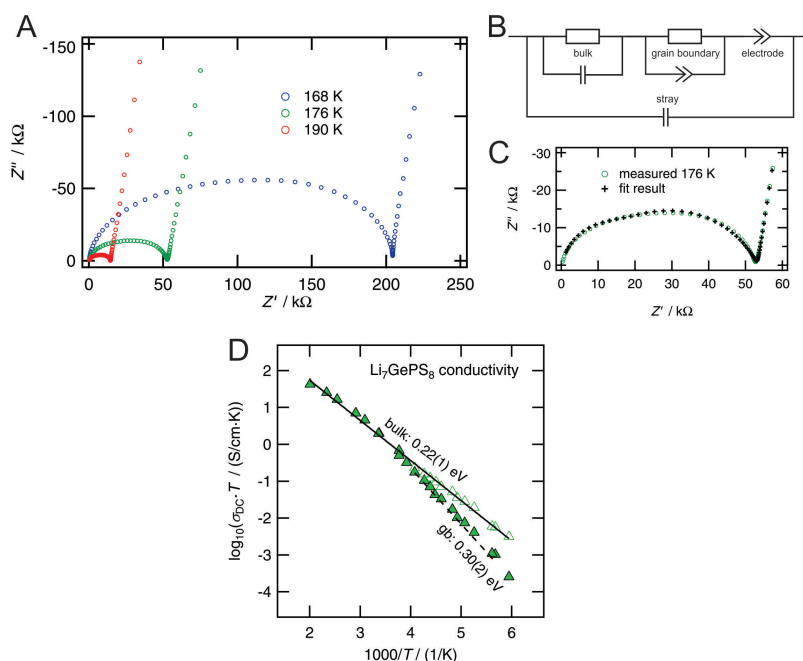


Fig. 4: Impedance spectroscopy on Li_7GePS_8 . (A): Nyquist impedance plot for selected temperatures. (B): Equivalent circuit used for the analysis. (>) denotes a constant phase element. (C): Fit result exemplarily shown for 176 K. (D): Full triangles: normalized total impedance as read out (model-independent) from the Nyquist plots shown in (A). Empty triangles: bulk impedance as obtained from the model-dependent fit.

Impedance spectroscopy probes charge transport on different length scales and can be used to study the contributions of bulk and grain boundary to the overall impedance. Fig. 4A shows typical Nyquist plots of impedance measurements of Li_7GePS_8 carried out at different temperatures. The total impedance of the measured pellet can be simply read out without a model-dependent analysis for all measurements (168...498 K). The values were normalized to the pellet size and the data are plotted in Fig. 4D as full green triangles. At room temperature, the conductivity amounts to approx. 7 mS/cm. The data follow a slope of approx. 0.2 eV above room temperature and a slope of 0.3 eV at low temperatures. This points to the presence of blocking grain boundaries (gb) at low temperatures while the room temperature conductivity is unaffected by grain boundary effects. This assumption is confirmed by estimating the capacity connected with the semicircles at low temperatures shown in Fig. 4A. The capacities obtained from the maxima of the semicircles are in the nF range being typical of gb processes but far too high for a bulk process. Indeed, the semicircle consists of two contributions which can be separated with a model-dependent fit analysis using the equivalent circuit shown in Fig. 4B. The capacities obtained from the fits were in the expected ranges (10-20 pF for the bulk capacity, 0.8-3 nF for the gb capacity, 2-3 μF for the electrode capacity). The stray capacity was in the low pF range and did not contribute to the overall result significantly. Therefore, it was kept constant in the fitting routine. As an example, the fit result and the measured data for 176 K are shown in Fig. 4C. The bulk conductivities extracted from the fitting analysis are included in Fig. 4D as open green triangles. The high-temperature total impedance and the low-temperature bulk impedance together nicely follow an Arrhenius behavior with an activation energy of 0.22(1) eV. The gb contribution, which plays a significant role below 250 K, is activated with 0.30(2) eV.